Fracture Mechanics of Concrete and Concrete Structures -
Recent Advances in Fracture Mechanics of Concrete - B. H. Oh, et al.(eds)


# Discontinuous cell method (DCM) for cohesive fracture propagation

G. Cusatis & E. A. Schauffert
*Rensselaer Polytechnic Institute, Troy (NY), USA*

ABSTRACT: This paper presents the formulation of the Discontinuous Cell Method (DCM) for the simulation of fracture propagation in homogeneous cohesive solids. Solid volumes are discretized by using Delaunay triangulation and its dual Voronoi tessellation. Rigid body kinematics of each Voronoi cell is adopted to approximate the displacement field. Weak forms of both equilibrium and compatibility Equations are used to derive the discretized DCM Equations. Elastic analyses and fracture simulations are carried out to investigate convergence and accuracy of the proposed method.

## 1 INTRODUCTION

A quantitative investigation of cohesive fracture propagation necessitates an accurate description of various fracture phenomena including: crack initiation; propagation along complex three-dimensional paths; interaction and coalescence of distributed multi-cracks into localized continuous cracks; temperature and humidity effects; loading rate effects; effect of the confining pressure; and interaction between fractured and unfractured material.

The classical finite element (FE) method, although it has been used traditionally to address some of these aspects, is inherently incapable of modeling the displacement discontinuities associated with fracture. To address this issue, advanced computational technologies have been developed in the recent past.

First, the embedded discontinuities methods (EDM) were proposed to handle displacement discontinuity within finite elements. In these methods the crack is represented by a narrow band of high strain, which is embedded in the element and can be arbitrarily aligned. Many different EDM formulations can be found in the literature and a comprehensive comparative study of these formulations appears in Jirásek (2000). The most common drawbacks of EDM formulations are stress locking (spurious stress transfer between the crack surfaces), inconsistency between the stress at the crack interface and the stress in the bulk of the material, and mesh sensitivity (where the crack path depends upon mesh alignment and refinement).

A method that does not experience stress locking and reduces mesh sensitivity is the extended finite element method (XFEM). The XFEM, first introduced to model cracks by Belytschko & Black (1999), exploits the partition of unity property of FE shape functions. This property enables discontinuous terms to be incorporated locally in the displacement field without the need of topology changes in the initial (uncracked) mesh. The XFEM has been successfully applied to a wide variety of problems (Moes et al. 1999, Dolbow et al. 2000, Belytschko et al. 2001, Belytschko et al. 2003). The drawbacks of this method are that the implementation into existing FE codes is not straightforward, the insertion of additional degrees of freedoms is required *on-the-fly* to describe the discontinuous enrichment, and complex quadrature routines are necessary to integrate discontinuous integrands.

Another approach widely used for the simulation of cohesive fracture is based on the adoption of cohesive zero-thickness finite elements located at the interface between the usual finite elements that discretize the body of interest (Camacho & Ortiz 1996, Ortiz & Pandolfi 1999). This method, even if its implementation is relatively straightforward, tends to be computationally intensive because of the large number of nodes that are needed to allow fracturing at each element interface. Furthermore, in the elastic phase the zero-thickness finite elements require the definition of an artificial stiffness to ensure inter-element compatibility. This stiffness usually deteriorates the accuracy and rate of convergence of the numerical solution and it may cause numerical instability. To avoid this problem, algorithms have been proposed in the literature (Pandolfi & Ortiz 2002) for the dynamic insertion of cohesive fractures into FE meshes. The dynamic insertion works reasonably well in high speed dynamic applications but is not adequate for quasi-static applications and leads to inaccurate stress calculations along the crack path.

An attractive alternative to the aforementioned approaches is the adoption of discrete models (parti-

cle and lattice models), which replace the continuum *a priori* by a system of rigid elements that interact by means of linear or nonlinear springs. These models were first developed to describe the behavior of particulate materials (Cundall & Strack 1979) and later adapted to simulate cemented materials (Bažant et al. 1990, Schlangen & VanMier 1992, Bolander & Saito 1998, Bolander et al. 1999, Bolander et al. 2000, Lilliu & Van Mier 2003, Cusatis et al. 2003a,b, Cusatis et al. 2006, Cusatis & Cedolin 2006, Cusatis at al. 2007a,b, Cusatis et al. 2008).

Discrete models can realistically simulate fracture propagation without suffering from the aforementioned typical drawbacks of other computational technologies. The effectiveness and the robustness of the method are ensured by the fact that: a) their kinematics naturally handle displacement discontinuities; b) the crack opening at a certain point depends upon the displacements of only two nodes of the mesh; and c) the constitutive law for the fracturing behavior is vectorial. Despite these advantages the general adoption of these methods to simulate fracture propagation in continuous media has been quite limited because of various drawbacks in the uncracked phase, including: 1) the stiffness of the springs is defined through a heuristic (trial-and-error) characterization; 2) various elastic phenomena, such as the Poisson effect, cannot be reproduced exactly; 3) the convergence of the numerical scheme to the continuum solution cannot be proved; 4) amalgamation with classical tensorial constitutive laws is not possible; and 5) spurious numerical heterogeneity (not related to the internal structure of the material) is inherently associated with these methods.

The Discontinuous Cell Method (DCM) presented in this paper provides a unified framework between discrete models and continuum based methods. The DCM formulation can potentially avoid most of the aforementioned shortcomings affecting current computational methods for cohesive fracture.

## 2 WEAK FORMS OF EQUILIBRIUM AND COMPATIBILITY

Within the assumptions of the first order theory, static behavior of continuous media can be expressed as:

$$\frac{\partial \sigma_{ij}}{\partial x_j} + f_{0i} = 0 \;\; ; \;\; \mathbf{x} \in \Omega \tag{1}$$

$$\varepsilon_{ij} - \frac{1}{2}\left( \frac{\partial u_i}{\partial x_j} + \frac{\partial u_j}{\partial x_i} \right) = 0 \;\; ; \;\; \mathbf{x} \in \Omega \tag{2}$$

$$\sigma_{ij} - F_{ij}(\varepsilon_{kl}) = 0 \tag{3}$$

where $\sigma_{ij}$ is the stress tensor, $f_{0i}$ represent body forces, $\varepsilon_{ij}$ is the strain tensor, $u_i$ is the displacement field, $\mathbf{x}=[x_1\ x_2\ x_3]^T$ is the position vector, and $\Omega$ is the solid volume. Equations 1, 2, and 3 represent equilibrium, compatibility, and constitutive Equations, respectively. It is noted here that unless otherwise indicated, index summation convention is used throughout this text.

The system of Equations 1, 2, and 3 can be integrated once essential ($u_i$-$u_{0i}$=0; $\mathbf{x}\in\Gamma_u$) and/or natural ($\sigma_{ij}n_i$-$t_{0i}$=0; $\mathbf{x}\in\Gamma_t$) boundary conditions are assigned. $\Gamma=\Gamma_u+\Gamma_t$ is the boundary of $\Omega$; $n_i$ is the outward normal to $\Gamma$, and $u_{0i}$, $t_{0i}$ are displacements and tractions, respectively, given on $\Gamma$.

By integrating Equations 1 and 2 over the volume $\Omega$ and by using Green's theorem one can obtain the weak forms of equilibrium and compatibility, which read:

$$\int_\Omega \sigma_{ij}\delta\varepsilon_{ij}\,\mathrm{d}\Omega + \int_{\Gamma_0} t_i \left[\!\left[\delta u_i\right]\!\right]\mathrm{d}\Gamma = \int_\Omega f_{0i}\delta u_i\,\mathrm{d}\Omega + \int_{\Gamma_t} t_{0i}\delta u_i\,\mathrm{d}\Gamma \quad \forall\,\delta u_i \tag{4}$$

and

$$\int_\Omega \varepsilon_{ij}\delta\sigma_{ij}\,\mathrm{d}\Omega + \int_{\Gamma_0} \left[\!\left[u_i\right]\!\right]\delta t_i\,\mathrm{d}\Gamma = \int_{\Gamma_t} u_i\delta t_i\,\mathrm{d}\Gamma \quad \forall\,\delta\sigma_{ij} \tag{5}$$

where homogeneous essential boundary conditions are considered for simplicity; and $\delta t_i=\delta\sigma_{ij}n_i$, $\delta\varepsilon_{ij}=0.5(\delta u_{i,j}+\delta u_{j,i})$, and $\delta u_i$, $\delta\sigma_{ij}$ are appropriate test functions which satisfy homogeneous essential boundary conditions and homogeneous equilibrium Equations (self-equilibrated stresses), respectively. In Equations 4 and 5, the displacements $u_i$ and the test functions $\delta u_i$ are allowed to be discontinuous on the oriented surface $\Gamma_0$. The jump of $\mathbf{u}$ and $\delta\mathbf{u}$ across $\Gamma_0$ are defined as:

$$\left[\!\left[\mathbf{u}\right]\!\right] = \mathbf{u}^+ - \mathbf{u}^-; \quad \left[\!\left[\delta\mathbf{u}\right]\!\right] = \delta\mathbf{u}^+ - \delta\mathbf{u}^- \tag{6}$$

where $\mathbf{u}^+$ and $\delta\mathbf{u}^+$ are the displacements and the test functions on the positive side of $\Gamma_0$, and $\mathbf{u}^-$ and $\delta\mathbf{u}^-$ are the same quantities on the negative side of $\Gamma_0$.

## 3 DISCONTINUOUS CELL METHOD (DCM)

Consider a discretization of volume $\Omega$ obtained by a Delaunay triangulation (tetrahedralization in 3D) and its dual Voronoi tessellation (Fig. 1).

The discretizised weak equilibrium and compatibility Equations for one triangle (tetrahedron in 3D) of the mesh can be expressed as follows:

$$\int_{\Omega^e} \sigma_{ij}^h\delta\varepsilon_{ij}^h\,\mathrm{d}\Omega + \int_{\Gamma_0^e} t_i^h \left[\!\left[\delta u_i^h\right]\!\right]\mathrm{d}\Gamma = \int_{\Omega^e} f_{0i}\delta u_i^h\,\mathrm{d}\Omega + \int_{\Gamma^e} t_i^h\delta u_i^h\,\mathrm{d}\Gamma \tag{7}$$

and

$$\int_{\Omega^e} \varepsilon_{ij}^h \delta\sigma_{ij}^h \, \mathrm{d}\,\Omega + \int_{\Gamma_0^e} \left[\!\left[ u_i^h \right]\!\right] \delta t_i^h \, \mathrm{d}\,\Gamma = \int_{\Gamma^e} u_i^h \delta t_i^h \, \mathrm{d}\,\Gamma \quad (8)$$

where $t^h{}_i=\sigma^h{}_{ij}n_i$, $\delta t^h{}_i=\delta\sigma^h{}_{ij}n_i$, $\delta\varepsilon^h{}_{ij}=0.5(\delta u^h{}_{i,j}+\delta u^h{}_{j,i})$, and $\varepsilon^h{}_{ij}=0.5(u^h{}_{i,j}+u^h{}_{j,i})$. Moreover, $\sigma^h{}_{ij}$ is an approximation of the actual stress tensor, $u^h{}_i$ is an approximation of the actual displacement field, and $\delta u^h{}_i$ and $\delta\sigma^h{}_{ij}$ are finite sets of orthogonal functions (basis functions) selected in the same space as the approximating functions (Galerkin approach). The functions $u^h{}_i$ and $\delta u^h{}_i$ are assumed to be discontinuous on the surface $\Gamma_{e0}$ which is defined by the union of the facets $\Gamma^k{}_0$ (triangles in 3D and line segments in 2D) forming the boundaries of each Voroni cell in the mesh.

The DCM formulation is based on the following selection of the basis functions:

$$\mathbf{u}^h(\mathbf{x}) = \mathbf{u}_I + \left(\mathbf{x}-\mathbf{x}_I\right)\times\boldsymbol{\theta}_I \quad \text{for} \quad \mathbf{x}\in\Omega_I \quad (9)$$

where $\Omega_I$ is the Voronoi cell associated with node $I$, and

$$\mathbf{t}^h(\mathbf{x}) = \mathbf{t}_k \quad \text{for} \quad \mathbf{x}\in\Gamma_0^k \quad (10)$$

where $\mathbf{u}_I$ and $\boldsymbol{\theta}_I$ are the nodal displacements and rotations (degrees of freedom).

By introducing Equations 9 and 10 into Equations 7 and 8, and after some mathematical manipulation, one obtains:

$$\sum_{k\in\Gamma_0^e} A_{0k} t_{ki} \delta w_{ki} = \int_{\Omega^e} f_{0i} \delta u_i^h \, \mathrm{d}\,\Omega + \int_{\Gamma^e} t_i^h \delta u_i^h \, \mathrm{d}\,\Gamma \quad (11)$$

and

$$\mathbf{w}_k \overset{\text{def}}{=} \frac{1}{A_{0k}} \int_{\Gamma_0^k} \left[\!\left[ \mathbf{u}^h \right]\!\right] \mathrm{d}\,\Gamma = \left[\!\left[ \mathbf{u}_C^h \right]\!\right]_{\Gamma_0^k} \quad (12)$$

where $A_{0k}$ is the area of the facet $\Gamma^k{}_0$ and $u_{Ci}{}^h$ is the displacement at the centroid $C$ of the facet $\Gamma^k{}_0$.

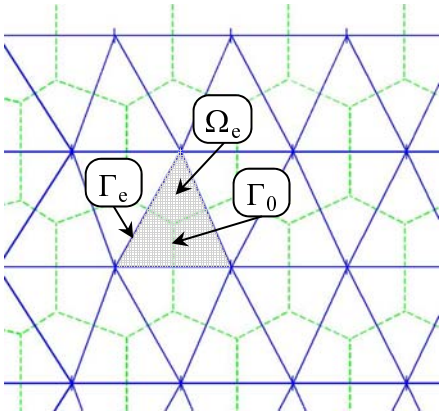

Figure 1. Delaunay triangulation and Voronoi tessellation.

Finally, combining Equations 11 and 12, and summing up the contributions of all elements in the mesh, one obtains a system of algebraic Equations (coinciding with the equilibrium Equations of the Voronoi cells) which allows for the computation of the nodal degrees of freedom once a relationship between the tractions $t_{ki}$ and the openings $w_{ki}$ is established. This relationship needs to be determined on the basis of the constitutive Equations.

## 4 ELASTIC BEHAVIOR

For a homogeneous and isotropic elastic medium, the constitutive law can be expressed as:

$$\sigma_{ij} = E_V \varepsilon_V \delta_{ij} + E_D \varepsilon_{D,ij} \quad (13)$$

where $\varepsilon_V=\varepsilon_{ii}/3$=volumetric strain, $\delta_{ij}$=Kronecker delta, $\varepsilon_{D,ij}=\varepsilon_{ij}-\varepsilon_V\delta_{ij}$=deviatoric strain tensor, $E_V=E/(1-2\nu)$=volumetric modulus, $E_D=E/(1+\nu)$=deviatoric modulus, $E$=Young's modulus, and $\nu$=Poisson's ratio.

By considering an average strain tensor in an element $\Omega^e$, one can obtain the relationship between the tractions $t_{ki}$ and the openings $w_{ki}$ by requiring that for a virtual variation of the stress tensor and facet tractions, the virtual complementary energy associated with the average strain equals the one associated with the openings $w_{ki}$:

$$\int_{\Omega^e} \overline{\varepsilon}_{ij} \delta\sigma_{ij} \, \mathrm{d}\,\Omega = \sum_{k\in\Gamma_0^e} A_{0k} w_{ki} \delta t_{ki} \quad (14)$$

With the appropriate choice of $\delta\sigma_{ij}$ and some mathematical manipulation, one can obtain:

$$\mathbf{t}_k = t_{Nk}\mathbf{n}_k + t_{Mk}\mathbf{m}_k + t_{Lk}\mathbf{l}_k \quad (15)$$

$$t_{Nk} = \frac{E_V - E_D}{3\alpha_\nu V^e} \sum_{k\in\Gamma_0^e} A_{0k} w_{Nk} + \frac{E_D w_{Nk}}{H_k} \quad (16)$$

$$t_{Mk} = \frac{E_D w_{Mk}}{H_k}; \quad t_{Lk} = \frac{E_D w_{Lk}}{H_k} \quad (17)$$

where $V_e$=element volume; $w_{Nk}=\mathbf{n}_k{}^{\mathrm{T}}\mathbf{w}_k$, $w_{Mk}=\mathbf{m}_k{}^{\mathrm{T}}\mathbf{w}_k$, and $w_{Mk}=\mathbf{l}_k{}^{\mathrm{T}}\mathbf{w}_k$ are the opening components orthogonal and tangential, respectively, to the facet $\Gamma^k{}_0$; $\mathbf{n}_k$, $\mathbf{m}_k$, and $\mathbf{l}_k$ are unit vectors orthogonal and tangential, respectively, to the facet $\Gamma^k{}_0$; and $H_k$ is the length of the element edge attached to the facet $\Gamma^k{}_0$ (Fig. 2). The parameter $\alpha_\nu$ is equal to 1 for three-dimensional and two-dimensional plane strain states whereas is equal to $(1-\nu)/(1-2\nu)$ for two-dimensional plane stress states.

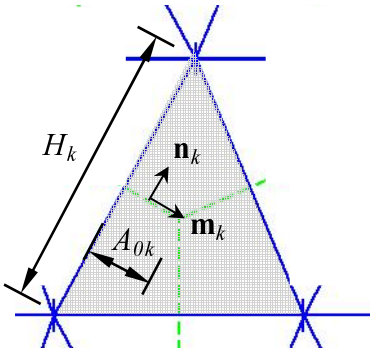


Figure 2. Facet area, edge length, and facet unit vectors.

Numerical experiments carried out in this study show that the 2D DCM triangle passes the patch test and it is able to reproduce exactly uniform strain and stress fields.

Furthermore, in order to study the convergence of the present method to the exact elastic solution, a classical cantilever beam test (Hughes 2000) was simulated by using six different meshes at various levels of refinement. The simulated beam was characterized by a length-to-depth ratio equal to 4. Figure 3 shows the coarsest mesh (132 elements) and the finest mesh (1958 elements) used in the convergence study. For comparison, the same numerical simulations were performed using a standard constant strain triangular (CST) finite element. All the computations were carried out under plain strain conditions, with a Poisson's ratio of 0.3.

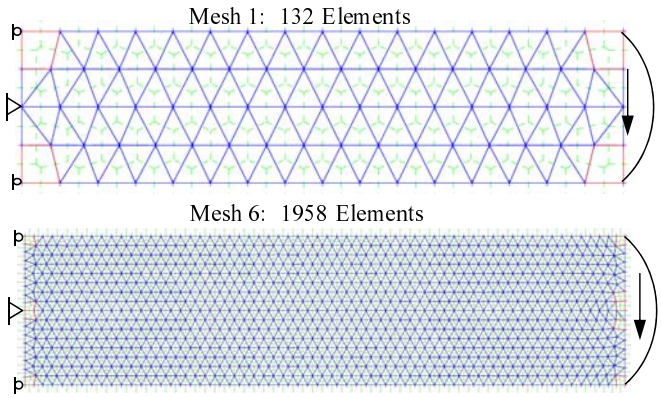


Figure 3. Coarsest (top) and finest (bottom) mesh used for the convergence study.

Figure 4 presents the results of the convergence study. In the top, one can see the percentage error for the total elastic energy as a function of the inverse of square root of the number of elements (proportional to characteristic element size). The bottom part of the figure reports the numerical results in terms of the vertical displacement at the tip of the cantilever beam. For the strain energy, the average convergence rates for the DCM and CST, respectively, are 1.76 and 1.99, and for the tip displacement they are 1.88 and 2.02. The theoretical convergence rate for the CST is 2 for both strain energy and tip deflection.

Although the convergence rates of the DCM and the CST are comparable, the DCM outperforms CST in terms of accuracy. The CST error in both strain energy and tip deflection is one order of magnitude higher than the DCM error. In terms of energy, for example, the DCM error ranges from 0.9% to 0.08% (coarsest to finest mesh), whereas the CST error ranges from 10% to 0.8%.

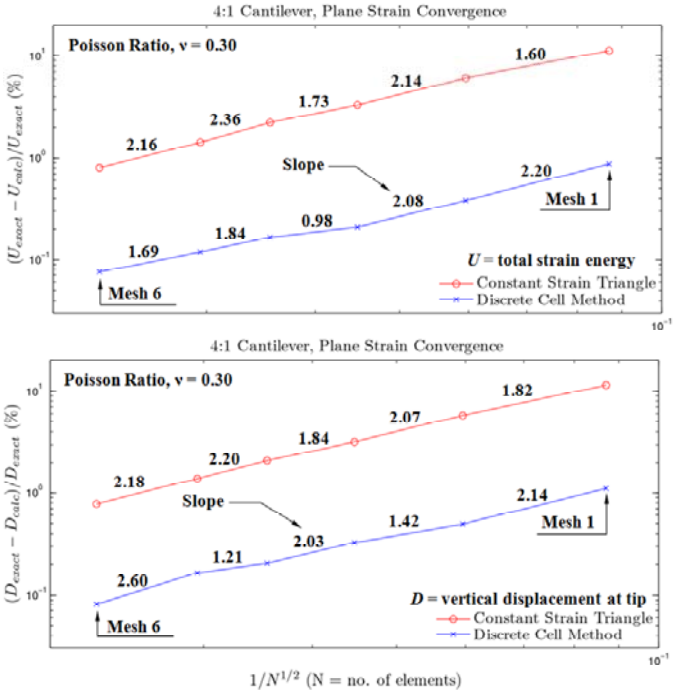


Figure 4. Convergence study in terms of energy (top) and tip displacement (bottom).

## 5 COHESIVE FRACTURING BEHAVIOR

The convergence study presented in the previous section demonstrates that DCM performs very well in the elastic regime. However, the most attractive feature of this method is the ability of easily accommodating the displacement discontinuity associated with fracture without suffering from the typical shortcomings of the classical finite element method, the limitations of typical particle models, or the complexity and the high computational cost of advanced finite element formulations (such as the extended finite element method and the embedded discontinuity method).

In this section a simple isotropic damage model is introduced in the DCM framework in order to simulate the initiation and propagation of quasi-brittle fracture.

According to classical damage mechanics and the DCM formulation for elasticity presented above, the facet tractions $t_{Nk}$ , $t_{Mk}$ and $t_{Lk}$ in a damaged material can be calculated as:

$$t_{Nk} = \left(1 - D_k\right)\left[\frac{E_V - E_D}{3\alpha_v V^e}\sum_{k\in\Gamma_0^e} A_{0k} w_{Nk} + \frac{E_D w_{Nk}}{H_k}\right] \qquad (18)$$

and

$$t_{Mk} = \left(1 - D_k\right)\frac{E_D w_{Mk}}{H_k}; \quad t_{Lk} = \left(1 - D_k\right)\frac{E_D w_{Lk}}{H_k} \qquad (19)$$

where $D_k$ is the damage parameter.

The evolution of the damage parameter is assumed to be governed by a history variable, the maximum effective strain ($\varepsilon_{\max}$), characterizing the overall amount of straining to which the material has been subjected during prior loading:

$$D_k = 1 - \frac{\varepsilon_t}{\varepsilon_{k,\max}}\exp\left[-\frac{\left\langle \varepsilon_{k,\max} - \varepsilon_t \right\rangle}{\varepsilon_{fk}}\right] \qquad (20)$$

where $\langle x\rangle = \max(0,x)$, $\varepsilon_t$ is a material parameter governing the onset of damage, and $\varepsilon_{fk}$ governs the damage evolution rate.

The maximum effective strain is defined as:

$$\varepsilon_{k,\max} = \frac{\sqrt{w_{Nk,\max}^2 + w_{Tk,\max}^2}}{H_k} \qquad (21)$$

$$w_{Nk,\max} = \max_{\tau \le t} w_{Nk}(\tau) \qquad (22)$$

$$w_{Tk,\max} = \max_{\tau \le t} \sqrt{w_{Mk}^2(\tau) + w_{Lk}^2(\tau)} \qquad (23)$$

In order to ensure convergence upon mesh refinement and to avoid spurious mesh sensitivity (Bažant & Oh 1984), one can write:

$$\varepsilon_{fk} = \frac{\varepsilon_t}{2}\left(\frac{l_t}{H_k} - 1\right) \qquad (24)$$

where $l_t$ is Hillerborg's characteristic length, which is assumed to be a material parameter.

In order to provide a demonstration of DCM ability to simulate cohesive fracture with this simple two-parameter model, the analysis of an experimental investigation that included the load versus displacement response for plain concrete in uniaxial tension was utilized (Li et al. 1998). As part of that investigation, panels with an approximate length of 240 mm and a cross-section of 100 mm by 20 mm were subjected to displacement controlled uniaxial tension. Two LDVTs, each with 120 mm length, were situated on both sides of the 100 mm width. The applied displacement was controlled by the LDVT that bounded the location of the fracture localization. The overall load versus displacement response was recorded, and is reproduced here in Figure 5.

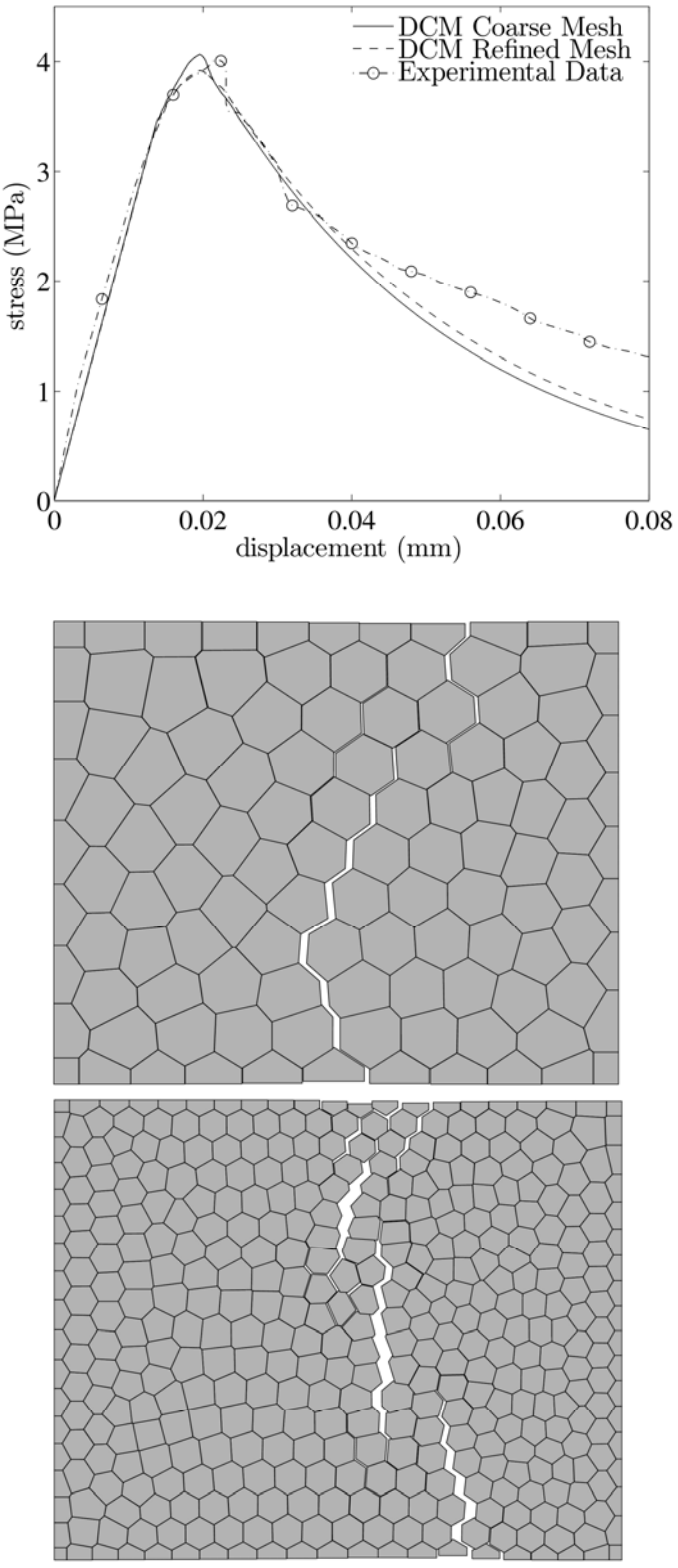


Figure 5. Load versus displacement curves (top), and fracture patterns: coarse mesh (center), refined mesh (bottom).

For the DCM simulation, a rectangular domain of 120 mm length, 100 mm width, and 20 mm out-of-plane thickness was used to model the portion of the experimental specimen that contained the fracture localization. Two triangulations of the domain were

considered: a coarse mesh with 190 elements, and a refined mesh with 746 elements. The discretizations were made as random as possible, subject to the desire for each mesh to have a certain characteristic element length. A non-zero velocity was applied to one end of the DCM mesh, and a zero-valued velocity was applied to the other. The load versus displacement response was calculated using an explicit-dynamic algorithm (Cusatis et al. 2003b) and using the same parameters for each mesh ($\varepsilon_t = 0.12\times10^{-3}$, $l_t$ = 700 mm).

Since the stress and strain are uniform in uncracked phase, some elements were made weaker in order to trigger localization. For these elements a 25% reduction of $\varepsilon_t$ and $l_t$ was used.

The resulting fracture patterns are shown in Figure 5 (center and bottom). They were visualized by amplifying the nodal displacements by a factor of 50, and plotting the displaced location of the rigid Voronoi cells.

The overall stress (load divided by the cross-sectional area) versus displacement curves are shown in Figure 5 (top). The responses of both meshes match well the experimental curve (Fig. 5, top) and, most importantly, there is no significant difference between the responses of the two meshes. This confirms that, within the DCM framework, the simple regularization model reported in Equation 24 is already enough to avoid mesh sensitivity and spurious localization.

## 6 DCM AND PARTICLE MODELS

DCM and classical particle models are basically governed by the same set of algebraic Equations expressing compatibility and equilibrium. This naturally follows from the adoption of rigid body kinematics which is common to the two approaches.

The difference between the two methods lies in the formulation of the constitutive law, namely in the relationship between facet tractions $\mathbf{t}_k$ and facet openings $\mathbf{w}_k$ (see Equations 16 and 17).

For classical particle models, which consider rigid particles connected with springs, this relationship can be expressed as:

$$t_{Nk} = \frac{E_N w_{Nk}}{H_k}; \quad t_{Mk} = \frac{E_T w_{Mk}}{H_k}; \quad t_{Lk} = \frac{E_T w_{Lk}}{H_k} \qquad (25)$$

where the normal elastic stiffness, $E_N$, and the tangential elastic stiffness, $E_T$, are assumed to be material properties.

By comparing Equations 16 and 17 with Equation 25, one can observe that an exact correspondence between the two formulations exists if, and only if, $E_N$=$E_T$=$E_D$ and $E_V$=$E_D$. These conditions correspond to an elastic material with zero Poisson's ratio (Bolander et al. 1999).

By properly setting the ratio between the normal and tangential stiffnesses, particle models can simulate an "average" non-zero Poisson's ratio (average in the sense that Poisson's ratio is defined by analyzing a finite, as opposed to an infinitesimal, volume of material. In this case, however, particle models feature an intrinsic heterogeneous response even under uniform solicitations (for additional discussion of this issue see also Bolander et al. 1999).

In conclusion, for non-zero Poisson's ratio the two formulations are fundamentally different and the key difference is that DCM accounts for the orthogonality of the deviatoric and volumetric deformation modes while classical particle models do not.

It must be mentioned here that the heterogeneous response of particle models is not necessarily a negative property and, actually, it is critical for their ability of handling automatically strain localization and crack initiation. It must be kept in mind, however, that in this case the size of the discretization cannot be user-defined but must be linked to the actual size of the material heterogeneity. Only under this condition can one consider the heterogeneous response of particle models to be a representation of the actual internal behavior of the material rather than a spurious numerical artifact.

## 7 CONCLUDING REMARKS

In this paper, the formulation of the Discontinuous Cell Method (DCM) has been outlined. A convergence study in the elastic regime shows that DCM converges to the exact continuum solution with a convergence rate that is comparable to that of constant strain triangles, but with accuracy that is one order of magnitude higher.

In addition, numerical simulations of fracture show that DCM easily simulates cohesive fracture propagation without the drawbacks of standard finite elements and without the complications of most recently formulated computational techniques.

Future DCM work will include the formulation of 2D quadrilateral elements, the formulation of 3D elements, and the application of the DCM framework to the numerical simulation of dynamic material fragmentation.

## 8 ACKNOWLEDGMENTS

Financial support under DTRA grant HDTRA1-09-1-0029 to Rensselaer Polytechnic Institute is gratefully acknowledged.

## REFERENCES


Bažant, Z.P. & Oh, B.H. 1984. Rock fracture via strain-softening finite elements. *Journal of Engineering Mechanics* 110(7): 1015-1035.

Bažant, Z.P., Tabarra, M.R., Kazemi, T., & Pijaudier-Cabot, G. 1990. Random particle model for fracture of aggregate or fiber composites. *J. Eng. Mech*. 116(8):1686-1705.

Belytschko, T. & Black, T. 1999. Elastic crack growth in finite elements with minimal remeshing. *International Journal for Numerical Methods in Engineering* 45(5):601-620.

Belytschko, T., Chen, H., Xu, J.X. & Zi, G. 2003. Dynamic crack propagation based on loss of hyperbolicity and a new discontinuous enrichment. *International Journal for Numerical Methods in Engineering* 58:1873-1905.

Belytschko, T., Moes, N., Usui, S. & Parimi, C. 2001. Arbitrary discontinuities in finite elements. *International Journal for Numerical Methods in Engineering* 50(4):993-1013.

Bolander, J.E. & Saito, S. 1998. Fracture analysis using spring network with random geometry. *Engng. Fracture Mech* 61(5-6):569-591.

Bolander, J.E., Hong, G.S. & Yoshitake, K. 2000. Structural concrete analysis using rigid-body-spring networks. *J. Comp. Aided Civil and Infrastructure Engng* 15:120-133.

Bolander, J.E., Yoshitake, K. & Thomure, J. 1999. Stress analysis using elastically uniform rigid-body-spring networks. *Journal of Structural Mechanics and Earthquake Engineering (JSCE)* 633(I-49):25-32.

Camacho, G.T. & Ortiz, M. 1996. Computational modeling of impact damage in brittle materials. *International Journal of Solids and Structures* 33:2899-2938.

Cundall, P.A. & Strack, ODL. 1979. A discrete numerical model for granular assemblies. *Geotechnique* 29:47-65.

Cusatis G., Mencarelli A., Pelessone D. & Baylot J.T. 2007a. Lattice Discrete Particle Model (LDPM): Formulation, Calibration, and Validation. *Electronic Proceedings (CD) of the International Symposium on the Interaction of the Effects of Munitions with Structures (ISIEMS) 12.1, Orlando, FL, September 17-21, 2007.*

Cusatis G., Mencarelli A., Pelessone D. & Baylot J.T. 2008. Lattice Discrete Particle Model (LDPM) for Fracture Dynamics and Rate Effect in Concrete. *Proceedings of the 2008 ASCE Structures Congress, Vancouver, April 24-26, 2008.*

Cusatis G., Pelessone D., Mencarelli A. & Baylot J.T. 2007b. Simulation of Reinforced Concrete Structures Under Blast And Penetration Through Lattice Discrete Particle Modeling. *Electronic Proceedings (CD) of IMECE 2007 - ASME International Mechanical Engineering Conferences & Exposition, Seattle, WA, November 11-15, 2007.*

Cusatis, G. & Cedolin, L. 2006. Two-scale analysis of concrete fracturing behavior. *Engng. Fracture Mech* 74:3-17.

Cusatis, G., Bažant, Z.P. & Cedolin, L. 2003a. Confinement-shear lattice model for concrete damage in tension and compression: I. Theory. *J. of Engrg. Mech. (ASCE)* 129(12):1439-1448.

Cusatis, G., Bažant, Z.P. & Cedolin, L. 2003b. Confinement-shear lattice model for concrete damage in tension and compression: II. Computation and validation. *J. of Engrg. Mech. (ASCE)* 129(12):1449-1458.

Cusatis, G., Bažant, Z.P., & Cedolin, L. 2006. Confinement-shear lattice model for fracture propagation in concrete. *Comput. Methods Appl. Mech. Engrg* 195:7154-7171.

Dolbow, J., Moes, N. & Belytschko, T. 2000. Discontinuous enrichment in finite elements with a partition of unity method. *Finite Elements in Analysis and Design* 36(3):235–260.

Hughes T.J.R. 2000. *The finite element method: linear static and dynamic finite element analysis*. Mineola, New York: Dover Publications.

Jirásek, M. 2000. Comparative study on finite elements with embedded discontinuities. *Computer Methods in Applied Mechanics and Engineering* 188:307-330.

Li, Z., Li, F., Chang, T.Y.P. & Mai, Y.W. 1998. Uniaxial tensile behavior of concrete reinforced with randomly distributed short fibers. *ACI Materials Journal* 95(5):564:574.

Lilliu G. & Van Mier J.G.M. 2003. 3D lattice type fracture model for concrete. *Engng. Fracture Mech* 70:927-941.

Moes, N., Dolbow, J. & Belytschko, T. 1999. A finite element method for crack growth without remeshing. *International Journal for Numerical Methods in Engineering* 46(1):133-150.

Ortiz, M. & Pandolfi, A. 1999. Finite-deformation irreversible cohesive elements for three-dimensional crack-propagation analysis. *International Journal for Numerical Methods in Engineering* 44:1267-1282.

Pandolfi, A. & Ortiz, M. 2002. An Efficient Adaptive Procedure for Three-Dimensional Fragmentation Simulations *Engineering with Computers*, 18(2):148-159.

Schlangen E. & Van Mier J.G.M. 1992. Shear fracture in cementitious composites, Part II: Numerical simulations. In Bažant, Z.P. (ed.), *Fracture mechanics of concrete structures*; *Proc. FraMCoS-1*. London: Elsevier.